ADVANCES IN ATMOSPHERIC SCIENCES, 2022

• Original Paper •

Effects of Dropsonde Data in Field Campaigns on Forecasts of Tropical Cyclones over the Western North Pacific in 2020 and the Role of CNOP Sensitivity※

Xiaohao QIN[1], Wansuo DUAN[*1,2], Pak-Wai CHAN[3], Boyu CHEN[4], and Kang-Ning HUANG[5]

[1]*State Key Laboratory of Numerical Modeling for Atmospheric Sciences and Geophysical Fluid Dynamics, Institute of Atmospheric Physics, Chinese Academy of Sciences, Beijing* 100029, *China*

[2]*Collaborative Innovation Center on Forecast and Evaluation of Meteorological Disasters, Nanjing University of Information Science and Technology, Nanjing* 210044, *China*

[3]*Hong Kong Observatory, Hong Kong, China*

[4]*Weather Forecasting Office, National Meteorological Center, China Meteorological Administration, Beijing* 100081, *China*

[5]*Research and Development Center, Central Weather Bureau, Taipei* 100006, *China*

(Received 9 May 2022; revised 22 July 2022; accepted 12 August 2022)

ABSTRACT

Valuable dropsonde data were obtained from multiple field campaigns targeting tropical cyclones, namely Higos, Nangka, Saudel, and Atsani, over the western North Pacific by the Hong Kong Observatory and Taiwan Central Weather Bureau in 2020. The conditional nonlinear optimal perturbation (CNOP) method has been utilized in real-time to identify the sensitive regions for targeting observations adhering to the procedure of real-time field campaigns for the first time. The observing system experiments were conducted to evaluate the effect of dropsonde data and CNOP sensitivity on TC forecasts in terms of track and intensity, using the Weather Research and Forecasting model. It is shown that the impact of assimilating all dropsonde data on both track and intensity forecasts is case-dependent. However, assimilation using only the dropsonde data inside the sensitive regions displays unanimously positive effects on both the track and intensity forecast, either of which obtains comparable benefits to or greatly reduces deterioration of the skill when assimilating all dropsonde data. Therefore, these results encourage us to further carry out targeting observations for the forecast of tropical cyclones according to CNOP sensitivity.

Key words: tropical cyclones, targeting observation, field campaign, CNOP sensitivity, dropsonde, intensity forecasts

Citation: Qin, X. H., W. S. Duan, P.-W. Chan, B. Y. Chen, and K.-N. Huang, 2022: Effects of dropsonde data in field campaigns on forecasts of tropical cyclones over the western North Pacific in 2020 and the role of CNOP sensitivity. *Adv. Atmos. Sci.*, https://doi.org/10.1007/s00376-022-2136-9.

Article Highlights:

- CNOP has been utilized for the first time to identify and produce the sensitive regions in real-time field campaigns for TCs in 2020.
- CNOP sensitivity helps obtain unanimously positive effects for both the track and intensity forecast compared to assimilating all dropsonde data.

1. Introduction

As an effective method to improve tropical cyclone (TC) forecasts, a targeting observational strategy aims at providing initial conditions that are as accurate as possible for numerical models by increasing additional observations in several localized but important sensitive regions and then assimilating them to the numerical model (Snyder, 1996). During the past several decades, targeting observations have demonstrated their roles in numerous field campaigns and subsequent forecasts (e.g., Burpee et al., 1996; Wu et al., 2005; Aberson, 2010; Weissmann et al., 2011; Feng and

※ This paper is a contribution to the special issue on the 14th International Conference on Mesoscale Convective Systems and High-Impact Weather.

* Corresponding author: Wansuo DUAN
Email: duanws@lasg.iap.ac.cn

Wang, 2019). From 2003 to 2009, 45 surveillance flights were conducted around 35 TCs over the western North Pacific (WNP), with 751 dropsondes released (Chou et al., 2011). Based on the 10 TCs in 2004, Wu et al. (2007) demonstrated that dropsonde data improved the 72-h track forecast of the ensemble mean of three global models by an average of 22%. In the summer of 2008, the Observing System Research and Predictability Experiment Pacific Asian Regional Campaign was conducted over the WNP. More than 1500 additional soundings were released during more than 500-h of flights for TCs Sinlaku (200813), Hagupit (200814), and Jangmi (200815). The data were found to improve the track forecasts by 20%–40% in both the modeling system of the National Center for Environmental Prediction global forecast and the Weather Research and Forecasting (WRF) model of the Korean Meteorological Agency. However, only modest improvements for forecasts of up to three days were observed in the systems of the European Centre for Medium-Range Weather Forecasts (ECMWF) and the Japan Meteorological Agency (Weissmann et al., 2011). More recently, the tropical cyclone intensity field campaign has provided high-resolution observations of TCs within the upper-level outflow, at an altitude of approximately 18 km and the inner-core (Braun et al., 2016; Black et al., 2017). With these data, the initial warm upper-level inner-core, as well as the related convection and latent heat release within the eyewall of Hurricane Patricia (2015), have been effectively simulated, which has contributed to improved forecasts of rapid intensification (Feng and Wang, 2019).

In the aforementioned field campaigns, major targeting observation techniques such as singular vectors (SVs), ensemble transform Kalman filters (ETKF), and adjoint-derived sensitivity steering vectors were utilized to identify the sensitive regions. All of these techniques utilize linear approximation to some degree. Then Mu et al. (2003, 2009) proposed a fully nonlinear method named conditional nonlinear optimal perturbation (CNOP) to identify the sensitive regions, which is a generalization of the leading singular vector to the nonlinear field. Observing system simulation experiments and observing system experiments (OSEs) were conducted for 7 and 20 TCs, respectively, to evaluate the effects of CNOP sensitivity on TC track forecasts (Qin and Mu, 2012; Chen et al., 2013). The results showed that the CNOP sensitivity demonstrated improvements of 13%–46% on TC track forecasts, although the effects are case-dependent; furthermore, CNOP sensitivity contributes similar improvements to the track forecasts as the ETKF, both of which are greater than that of the leading SV. However, all of the aforementioned evaluations for CNOP sensitivity are based on hindcasts initialized by the reanalysis data, which are available after the actual observing. The CNOP method has never been utilized in a real-time field campaign to provide the sensitive region in advance for targeting observations; moreover, little work has been done thus far on the effects of CNOP sensitivity on the TC intensity forecast. As a necessity, but with much larger uncertainties than the reanalysis data, the real-time forecasts should be utilized to provide the initial and boundary conditions for a numerical model to identify the sensitive regions ahead of the actual field campaigns. Therefore, the feasibility and validity of the identified sensitive regions in this instance should be evaluated in terms of their potential to improve the forecast of the TC's track and especially its intensity before widely deploying this application for targeting observation in field campaigns.

The model, CNOP method, and its application in the field campaign for TCs in 2020 are introduced in section 2. Section 3 illustrates the identified CNOP sensitive regions and their associated synoptic characteristics for each TC first, followed by the results of assimilating all dropsonde data, especially those inside the sensitive regions on TC track and intensity forecasts. Then the CNOP sensitivity is further applied to TC forecasts conducted under a finer, convection-permitting resolution. Section 4 displays the results before a summary and discussion are presented in section 5.

2. Model, CNOP method, and field campaign for TCs in 2020

In 2020, East Asia's main operational meteorology centers conducted many field campaigns targeting TCs over the South China Sea (SCS) and the WNP (Fig. 1). The CNOP method was utilized for the first time to identify the sensitive regions following the procedures of the real-time field campaign, which is based on the WRF model Version 3.6 (WRFV3.6) and its adjoint model.

2.1. *The WRFV3.6*

The WRFV3.6 conducts the forecasts with and without dropsonde data in the present study, which adopts the Kain-Frisch cumulus parameterization (Kain and Fritsch, 1993),

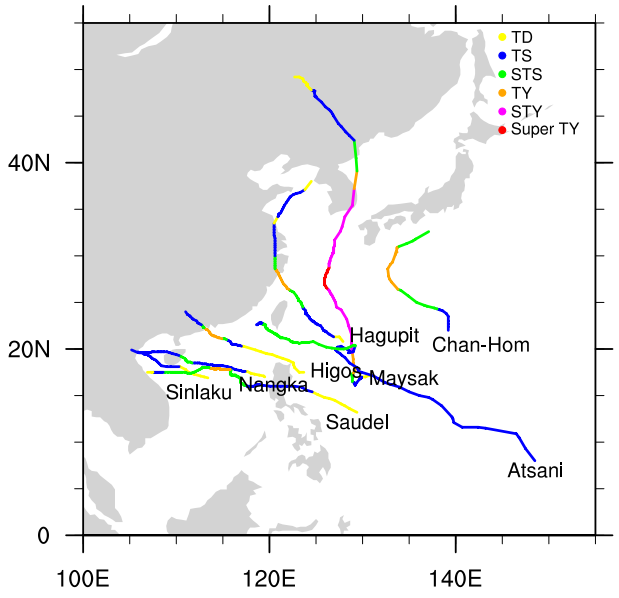

Fig. 1. Field campaigns on TCs over the western North Pacific in 2020. Different intensities of a tropical depression (TD), tropical storm (TS), severe tropical storm (STS), typhoon (TY), severe typhoon (STY), and super typhoon (Super TY) are indicated in corresponding colors.

Lin microphysics scheme (Lin et al., 1983), RRTMG for longwave and shortwave radiation schemes (Iacono et al., 2008), and Yonsei University planetary boundary layer parameterization scheme (Hong et al., 2006). All the model integrations are conducted in a single model domain of 228 × 228 grid points at a resolution of 30 km with 19 vertical eta levels (with a top of 20 hPa). The latest real-time deterministic forecasts from the ECMWF model at a resolution of 0.125° × 0.125° are used to provide the initial and boundary conditions for the model area.

In addition, the WRFV3.6 and its adjoint model are employed to identify the CNOP sensitive regions. Noting that only simplified parameterization schemes are available in the adjoint model (i.e., lscond microphysical scheme, surfdrag planetary boundary layer scheme, and ducu cumulus convective parameterization schemes), and its derived gradient fails to pass through an accuracy check for a much finer resolution (also see Qin et al., 2020), thus forcing us to use a resolution of 30 km to calculate the CNOP sensitivity in the present study. For this reason, we can justify using a resolution of 30 km in the aforementioned OSEs, based on which the evaluations are deemed reasonable.

2.2. *CNOP method*

The CNOP represents the initial error that can lead to the largest forecast error at a given prediction time. It is obtained by solving the following optimization equation with respect to the initial perturbations δx_0 using the spectral projected gradient 2 (SPG2) algorithm (Birgin et al., 2001):

$$\begin{cases} J(\delta x_0^*) = \max\limits_{\delta x_0^{\mathrm{T}} C_1 \delta x_0 \leqslant \beta} E^{\mathrm{T}} C_2 E \\ E = M(X_0 + \delta x_0) - M(X_0)\ , \end{cases} \tag{1}$$

where $M(X_0)$ and $M(X_0+\delta x_0)$ represent the forecasts initialized by X_0 and $X_0+\delta x_0$, respectively; the superscript T is the transpose; the coefficient matrices, C_1 and C_2, measures the initial perturbations δx_0 and its evolution $[M(X_0+\delta x_0)-M(X_0)]$, which are respectively determined according to the physical problems of interest and are defined here as the total energy over a horizontal area D from the surface ($\sigma = 1$) to a height of $\sigma = 0$ as in Eq (2); β limits the upper bound of the initial perturbations, which is pre-assigned according to the magnitude of the initial analysis error variance of each considered variable.

The total perturbation energy is given by Eq. (2):

$$C_{1,2} = \frac{1}{D}\int_D \int_0^1 \left[u'^2 + v'^2 + w'^2 + \frac{c_p}{T_r}\theta'^2 + \frac{L^2}{c_p T_r} q'^2 + \frac{g}{T_r R_a} p'^2 \right] \mathrm{d}\sigma \mathrm{d}D\ . \tag{2}$$

It is comprised of $[u', v', w', \theta', q', p']$, which respectively denotes the perturbations of the horizontal (u', v') and vertical (w') wind, potential temperature (θ'), mixing water ratio (q'), and pressure (p'). The contants are given as L= 2.5104 × 10^6 J kg^{-1}, c_p = 1005.7 J kg^{-1}, T_r = 270 K, and R_a =287.04 J kg^{-1} K^{-1}. It should be noted that the total perturbation energy associated with the vertical wind (w') is only accounted for by measuring the forecasts of $M(X_0+\delta x_0)$ and $M(X_0)$ (i.e., C_2 in Eq. 2), since any initial perturbation in w' cannot induce forecast differences in the simplified WRFV3.6.

In the calculation of CNOP, a first guess is assigned to the initial perturbation δx_0 which includes the components of the vector $[u', v', \theta', q', p']^{\mathrm{T}}$. Then the WRFV3.6 model is integrated forward with the initialization of $X_0+\delta x_0$ to obtain the forecast $M(X_0+\delta x_0)$ with the reference state $M(X_0)$ initialized at X_0 allowing for the cost function J to be calculated. The associated adjoint model of the WRFV3.6 is integrated backward to calculate the gradient of the cost function with respect to the initial perturbations, δx_0. The gradient here represents the fastest descending direction of the cost function. Based on the automatic and iterative forward and backward integrations in the WRFV3.6 and its adjoint model, which are respectively governed by the SPG2, the initial perturbation δx_0 is optimized and updated until the convergence condition is satisfied. Then the resultant initial perturbation δx_0^* is just the CNOP.

Once the CNOP comprised of $[u', v', \theta', q', p']$ is solved, the total perturbation energy is calculated using Eq. (2), which allows for the total perturbation energy values on the grid points to be sorted in descending order. The grid points with large values comprise the sensitive regions for CNOP sensitivity.

2.3. *The procedure for the TC field campaign in 2020*

Field campaigns targeting TCs over the WNP made great progress in 2020, in which the China Meteorological Administration (CMA), Hong Kong Observatory (HKO), and Taiwan Central Weather Bureau (CWB) played important roles. From mid-August to early October, the Numerical Prediction Center CMA, in collaboration with the Institute of Atmospheric Physics Chinese Academy of Sciences, the Department of Atmospheric and Oceanic Sciences of Fudan University, and the National Satellite Meteorological Center CMA, conducted targeting observation at 30-min intervals on TCs Higos (202007), Maysak (202009), and Chan-Hom (202014) using the Fengyun-4 satellite. These observations employed the CNOP method to identify sensitive regions, which is the first time that CNOP has been utilized in real-time field campaigns. In the same period, the CNOP sensitivities were also calculated for three SCS TCs (Higos 202007; Nangka 202016; and Saudel 202017) in the field campaigns conducted by the HKO. Especially on 12 October 2020, the Shanghai Typhoon Institute CMA, along with several other organizations, conducted a sea-land-air field campaign over the SCS to observe TC Nangka (202016), which allowed for the sensitive region identified 24-h in advance. Multiple observational platforms, such as satellites, unmanned aerial vehicles, unmanned sea surface vehicles, and vehicles, have been utilized in this field campaign. In addition, the CWB conducted another field campaign for TC Atsani (202020) in early November and gained valuable dropsonde data,

where the CNOP sensitivity is presently available. However, it was not considered in its real-time field campaign.

Taking TC Nangka (202016) as an example, the process of a field campaign is briefly illustrated in Fig. 2. A decision was made on 10 October (i.e., –54 h with respect to the actual observing time of 0 h) to conduct a field campaign on 12 October. At approximately 1900 UTC on 10 October (3 a.m. Beijing time on October 11), the latest deterministic forecasts over East Asia issued by the ECMWF, initialized at 1200 UTC on 10 October (i.e., –42 h) with forecast lead times from 0 h to 240 h at 3-h intervals, were produced and transferred to the terminal in the CMA. At this time, the identification of the sensitive regions was started using the CNOP method, which became available before approximately 0600 UTC on 11 October (i.e., –24 h). Thus, sufficient time (24-h from 0600 UTC on 11 October to 0600 UTC on 12 October) was reserved for the subsequent design of the exact observing locations and equipment preparation. With joint considerations of air traffic control, the airspace (i.e., flight forbidden outside) of the airplanes performing the missions, and the identified sensitive regions, the observations started at approximately 0600 UTC on 12 October (i.e., 0 h) and, subsequently, the resultant data was assimilated to the model after quality control.

The data quality control of dropsondes varies greatly from one dropsonde to another. There could also be a small duration of data loss within the data set of a dropsonde. Hence, auto quality control might not guarantee the high quality of data. As the number of dropsondes would not be large in each operation, manual quality control assisted with a web-based visualization tool was applied, allowing for suspicious observations to be discarded.

3. Evaluations

Of all TCs with field campaigns reported in Section 2, the Fengyun-4 data for TCs Higos (202007), Maysak (202009), and Chanhon (202014) have been separately investigated in another study (Feng et al., 2022) due to the peculiarity of satellite observations and associated assimilation. The dropsonde data collected for TCs Higos (202007), Nangka (202016), Saudel (202017), and Atsani (202020) also allowed for the CNOP sensitivity in the field campaigns to be evaluated as follows.

For the track forecasts, the distances between the forecast TC central positions and those from the best track data issued by the CMA (referred to as the BEST) denote the errors, which cover a 30-h period from the observing time at 1-h intervals. Regarding the intensity forecasts, two indicators are investigated: the minimum sea-level pressure and the maximum sustained near-surface wind associated with the TCs (hereafter referred to as $P_{\min}$ and $V_{\max}$, respectively), the errors of which are also obtained by comparing the forecasts with the BEST for the same period at 1-h intervals.

3.1. *The sensitive regions of targeting observation for TC forecasts*

As a synoptic system that lasts for several or more than ten days, a TC originates from and is influenced by different environmental systems. Therefore, the sensitive region for each TC forecast may be spatiotemporally dependent on the specific synoptic situation and even differ from time to time for the same TC. In this section, the sensitive regions and the synoptic characteristics they reveal are detailed for each individual TC.

3.1.1. *TC Higos (202007)*

The TC Higos (202007) originated east of Luzon Island on 16 August and moved northwestward into the SCS. It intensified to a typhoon at 1200 UTC on 18 August, within a distance of less than 200 km from the south coast of China. For this TC, we adopt the real-time forecasts issued by the ECMWF at 1200 UTC on 16 August to provide both the initial and boundary conditions for the WRF model and identify the CNOP sensitive region to be targeted at the observing time at 0600 UTC on 18 August. The identified sensitive region is shown in Fig. 3a, which covers the Bashi Channel, Taiwan Strait, and their adjacent lands. Combined with the forecast 500 hPa geopotential at 0600 UTC on 18 August, it is found that the subtropical high, which was centered over the Korean Peninsula and Japan, dominated the synoptic environment over the WNP at that time. As a much weaker system, the development of this TC was strongly dependent on the influence of the subtropical high near the border area between the subtropical high and the TC. Not surprisingly, the identified sensitive region is exactly located around this border area, where any change would likely induce a shift in the forecast track and intensity. We may infer that targeting observations in the sensitive region would be more probable to reduce the initial uncertainties there and further reduce forecast uncertainty in the area of concern (rectangle in Fig. 3a). From 0700 UTC to 0900 UTC on 18 August, the HKO released eight dropsondes (blue dots in Fig. 3a) from an aircraft. Only dropsonde No. 8 was inside and at the edge of the sensitive region due to an airspace issue.

3.1.2. *TC Nangka (202016)*

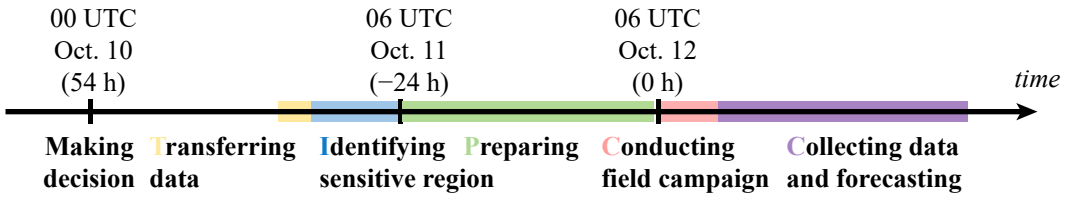

Fig. 2. Illustration of the field campaign for TC Nangka (202016).

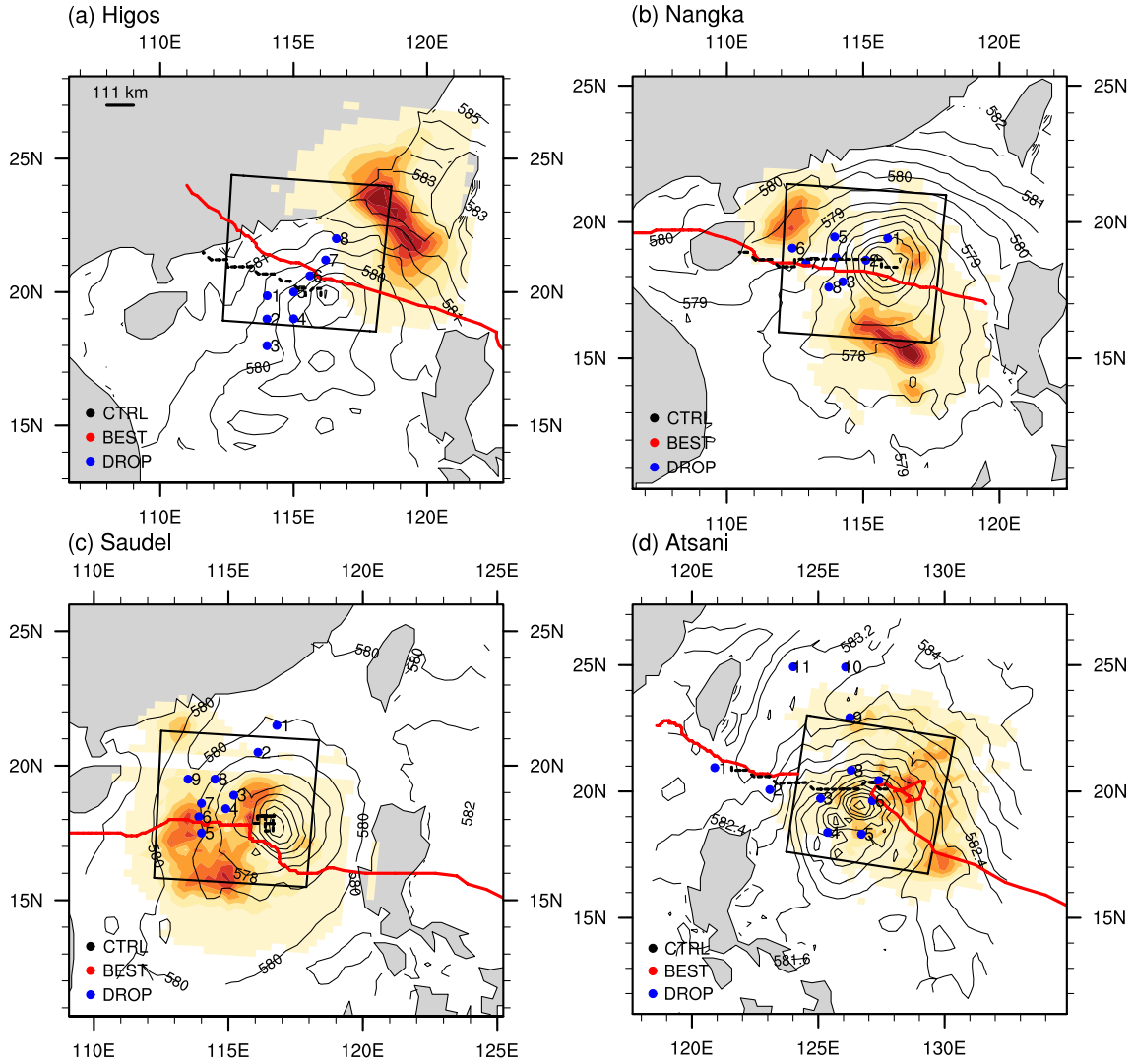

Fig. 3. Sensitive regions (shaded; the warmer, the more sensitive) identified by the CNOP method aiming at the forecasts in the verification area (small rectangle) and the geopotential (contour; 10^2 m^2 s^{-2}) at 500 hPa at 0600 UTC on 18 August, 0600 UTC on 12 October, 0600 UTC on 22 October, and 1800 UTC on 4 November for TC (a) Higos, (b) Nangka, (c) Saudel, and (d) Atsani, respectively. The best tracks (BEST) and forecast tracks (30-h) without any assimilation of dropsonde data (CTRL) are respectively indicated by the red solid and black dotted lines. The released dropsondes (DROP) are dotted in blue.

TC Nangka (202016), another SCS TC, formed in the west coastal area of Luzon Island. It moved west-northwestward and made landfall for the first time on Hainan Island at 1200 UTC on 13 October with an intensity of a severe tropical storm. After passing over the island, it moved over the ocean again for 17-h with no apparent variations in intensity. Then, it made a second landfall in Vietnam at approximately 1000 UTC on 14 October. Based on the forecasts issued by the ECMWF at 1200 UTC on 10 October, the sensitive region targeting the forecasts from 0600 UTC on 1200 October to 0600 UTC on 13 October was then identified. It shows that the eastern SCS, especially two local areas to the south and northwest of the storm, exhibit higher sensitivities (Fig. 3b). The forecast 500 hPa geopotential shows that a strong subtropical high and a monsoon trough were to the north and southwest of the TC at that time, respectively, indicating a close co-interaction between the TC and these two synoptic systems. On the one hand, the TC has to overcome the resistance from the subtropical high to the north if it were to move northward; on the other hand, it needs to maintain a continuous supply of moisture from the monsoon trough in the south if it were to intensify. Hence, it is very important to accurately depict the characteristics in these areas where the interaction between these synoptic systems and the TC occurred. These areas are coincident with the regions with higher sensitivity by the CNOP. From 0700 UTC to 0900 UTC on 12 October, the HKO released 13 dropsondes from an aircraft, 8 of which (blue dots in Fig. 3b) collected available data at multiple levels. All of these dropsondes appear to be either inside or at the edge of the sensitive

region.

3.1.3. *TC Saudel (202017)*

TC Saudel (202017) experienced a long lifetime of over 162-h. It originated over the ocean east of the Philippines, intensified slowly, and moved into the SCS after passing over the Philippines. It intensified again to a typhoon at 0700 UTC on 22 October and then moved directly north. At 1500 UTC on 22 October, TC Saudel made a sudden 90° turn to the west. For the rest of its lifetime, it moved westward until making landfall in Vietnam at 1800 UTC on 25 October. Based on the forecasts issued by the ECMWF at 1200 UTC on 20 October, the sensitive region is identified as the area around the TC itself, especially on its west side (Fig. 3c), which differs somewhat from the other two TCs previously discussed. These differences can also be seen from the 500 hPa forecast, from which it is evident that the TC was the only dominant synoptic system over this area at that time. Consequently, further development of the TC probably depended on itself, noting the absence of any synoptic systems that could have significantly influenced the TC. Hence, the region controlled by the TC is identified as the sensitive region by the CNOP. From 0800 UTC to 1000 UTC on 22 October, the HKO released ten dropsondes around the TC. All dropsondes except for one (blue dots in Fig. 3c) collected available data in the troposphere below 10.1 km. All nine available dropsondes fell inside the sensitive region.

3.1.4. *TC Atsani (202020)*

In contrast to the three TCs mentioned above, Atsani (202020) remained over the WNP for most of its lifetime. It formed over the ocean southeast of Guam at 1200 UTC on 29 October and moved northwestward until it approached the Bashi Channel at 1800 UTC on 2 November. Then, it abruptly made a 90° turn and revolved for another 51-h before moving northwestward again until its dissipation over the Taiwan Strait at 1200 UTC on 7 November. Based on the forecasts issued by the ECMWF at 0000 UTC on 3 November, the CNOP sensitive region targeting forecasts for the period 1800 UTC on 4 November to 1800 UTC on 5 November is indicated by the shaded area in Fig. 3d. It is clear that the environments, especially in the north and east, as well as in the area of the TC, exhibit more sensitivity than other areas. The forecast 500-hPa geopotential indicates that the ridge line of the subtropical high withdrew around 20°N, and the TC was to the southwest of the subtropical high, which resembled the synoptic situation of TC Higos (202007) discussed above. The identified sensitive region corresponds well with the border area between the southwestern of the subtropical high and the TC. Naturally, the flow there steered and dominated the subsequent development of the TC, from which the potential changes would induce the forecast uncertainty of the TC. Starting from 15 UTC on 4 November, the CWB released 13 dropsondes, among which the valid ones are represented by the blue dots in Fig. 3d. It is clear that dropsondes Nos. 3–9 are inside the sensitive region, while dropsondes Nos. 1, 2, 10, and 11 are not.

3.2. *Track forecasts and the role of CNOP sensitivity*

3.2.1. *TC Higos (202007)*

The forecast tracks of the four TCs and their forecast errors with respect to the BEST, including those without any assimilation and with all dropsonde data assimilated (referred to as CTRL and All, respectively), are shown as "Exp-30 km" in Fig. 4. TC Higos (202007) was forecasted in the CTRL to have a relatively slower translation speed, which led to its landfall behind the actual to the south and a position approximately 200 km west of the actual site. After assimilating all dropsonde data, neither the moving direction nor the translation speed changes obviously from that in the CTRL; furthermore, the average 30-h forecast error increases slightly by 4.9% compared with that in the CTRL (Fig. 4b). That is, assimilating all dropsondes does not positively affect the track forecast for this TC.

As mentioned in section 3.1, only dropsonde No. 8 for this TC was released into the sensitive region, while the other seven were outside. Compared to the other seven, dropsonde No. 8 can better reflect the effect of CNOP sensitivity. Hence, another OSE is conducted with the same experimental design as above but assimilating only the dropsonde data inside the sensitive region, i.e., the No. 8, referred to as "Sen" below for simplification. In comparison, the forecast translation speed is faster than those in both CTRL and All, which is the closest to the BEST out of the three forecasts. However, the forecast moving direction shows no substantial variations from the other two, leading to a further westward landfall site. Nevertheless, the similar translation speed to the actual improves the forecast, reducing the average forecast error by 5.4% in the Sen. This result indicates that targeting observation according to CNOP sensitivity not only overcomes the deterioration as that in All but slightly improves upon the track forecast skill for this TC.

3.2.2. *TC Nangka (202016)*

Compared to the relatively straightforward actual track shown in Fig. 4e, the forecast track in the CTRL is crooked. In consequence, it does not make an accurate landfall in this 30-h, which maintains a forecast error below 100 km during most of the period. Similar to Higos (202007), an assimilation of all the data has little effect on either the moving direction or the translation speed, which apparently causes an increase of the average track forecast error by 4.7% compared with that in the CTRL (Fig. 4f). It is noted that all dropsondes for this TC were released inside the sensitive region. Hence, the effects illustrated in All completely represent that of CNOP sensitivity. That is, the CNOP sensitivity fails to upgrade the track forecast in CTRL for this TC.

3.2.3. *TC Saudel (202017)*

Obvious track differences between the BEST and CTRL are revealed for this TC (Fig. 4i). It is obvious that the TC in the CTRL is stagnant around its initial location for the subsequent 30-h, which maintains relatively large

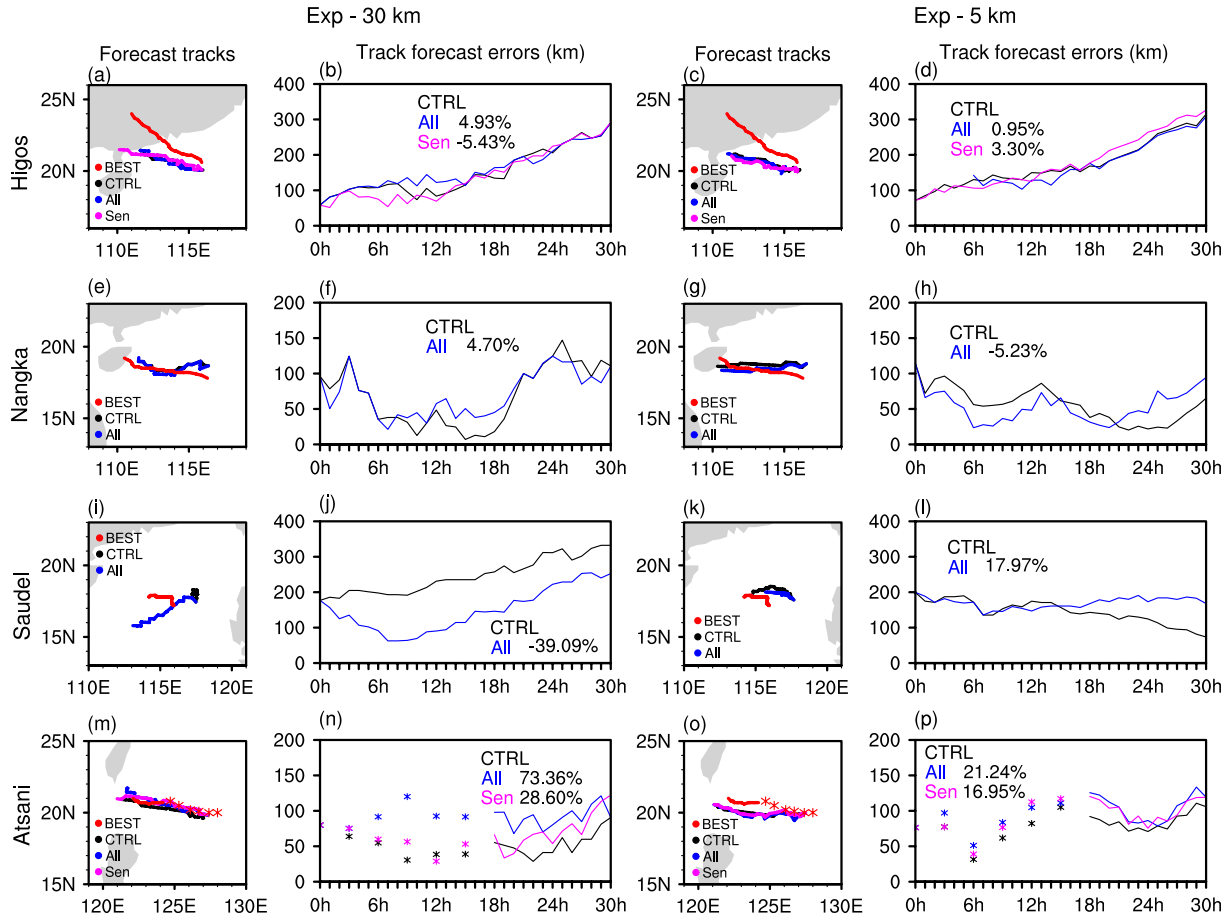

Fig. 4. An evaluation of dropsonde data and CNOP sensitivity with a resolution of 30 km (Exp-30 km) and 5 km (Exp-5 km). In each panel, the left shows the best track (red), forecast tracks in the CTRL (black), after assimilating all dropsonde data (All; blue), and those inside the CNOP sensitive regions (Sen; magenta); and the right shows the track forecast errors (km) in the CTRL (black), after assimilating all dropsonde data (All; blue), and those inside the CNOP sensitive regions (Sen; magenta). The relative forecast errors with respect to the CTRL are denoted as the percentages.

track forecast errors (≥200 km) from the BEST for this period. However, significant variations occur in the forecast track when all dropsonde data are assimilated, which makes the TC rapidly move towards the BEST but then deviate from it after nine hours. Despite this behavior, the average forecast error is reduced by 39.1% compared with that in the CTRL (Fig. 4j), representing a substantial improvement to the track forecast. Similar to TC Nangka (202016), all dropsondes were released inside the sensitive region. Hence, the CNOP sensitivity greatly improves upon the track forecasts relative to the CTRL for this TC.

3.2.4. *TC Atsani (202020)*

For TC Atsani (202020), the forecast track in the CTRL is close to the BEST from 1800 UTC on 4 November to 0000 UTC on 6 November (Fig. 4m). In this situation, the forecast error was generally maintained at around 50 km, which indicates a good track forecast. After assimilating all dropsonde data, there are no obvious differences in the track from that of the CTRL; however, the average track forecast error increases significantly by 73.4% (Fig. 4n). This is probably due to the small absolute track forecast error in the CTRL, where an absolute error of 50 km denotes twice in the relative error. Nevertheless, it is a fact that assimilating all dropsondes data causes deterioration for this TC.

As mentioned above, seven dropsondes (Nos. 3–9) were released inside the sensitive region, while the other four (Nos. 1, 2, 10, and 11) were outside. Hence, the effect of assimilating the seven dropsonde data is also shown in Figs. 4m and 4n. The forecast track does not show obvious differences from either the BEST or that in the CTRL (and All) since they all cluster together and maintain a parallel track during this 30-h. However, the average deterioration is reduced from 73.4% in All to 28.6% in Sen. This result indicates again that CNOP sensitivity greatly helps in reducing the deterioration caused by assimilating all dropsonde data for this TC, which displays its advantages in targeting observations.

3.3. *Intensity forecasts and role of CNOP sensitivity*

3.3.1. *TC Higos (202007)*

The forecast intensity in the CTRL maintains a relatively steady $P_{\min}$ ($V_{\max}$) around 1000 hPa (14 m s^{-1}) in this 30-h

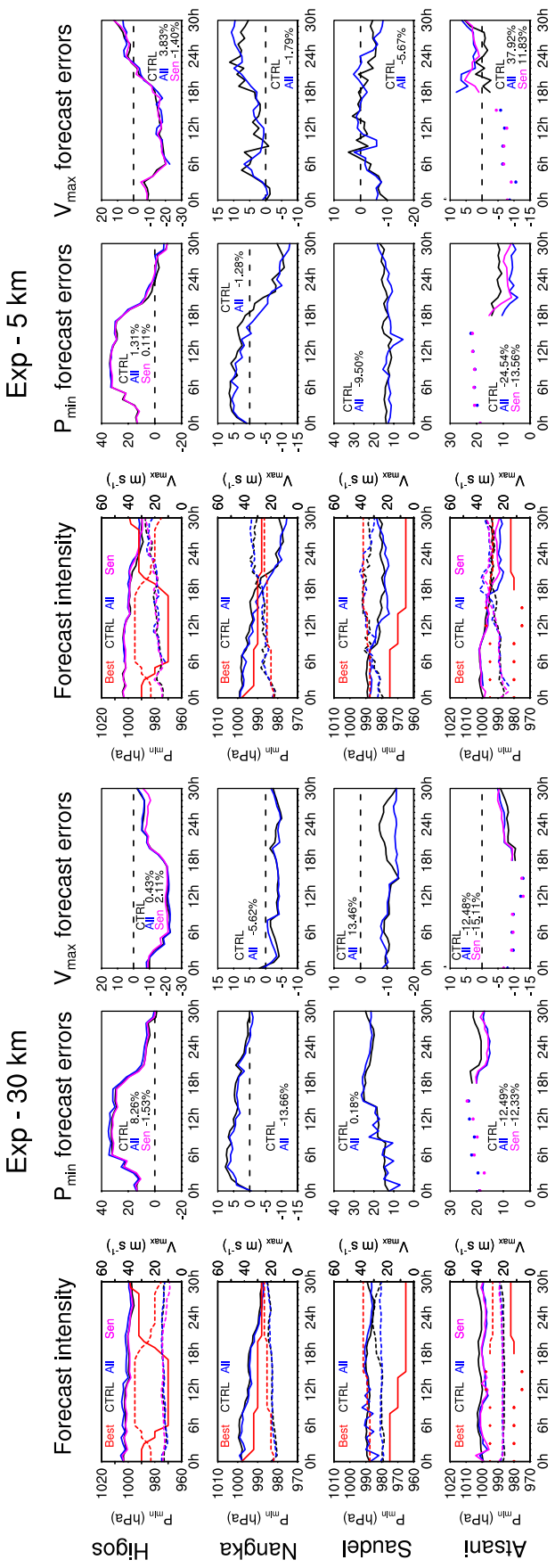

Fig. 5. Same as Fig. 4 but for intensity.

(Fig. 5), which fails to predict the actual intensification occurring in the former 6-h and displays great intensity errors. This is possibly due to the large track deviation from the actual one. Similar to the insignificant variations in the forecast track after assimilating all dropsonde data, the forecast intensity in All shows modest differences from that in the CTRL, which increases the average forecast errors by 8.3% for the P_{min}. In comparison, the impacts of all dropsondes are nearly neutral on the V_{max}. Combining these two indicators, it is indicated that the dropsonde data does not aid the improvement of the corresponding intensity forecast skill for this TC.

Different from the averaged negative effect of all dropsonde data on the P_{min} forecast, assimilating the single dropsonde data from No. 8 in the sensitive area reduces the average forecast error in the CTRL by 1.5%. Numerically, this is trivial; however, it transforms the general deterioration caused by all dropsondes to a slight improvement, indicating CNOP sensitivity advantages for this TC. Nevertheless, the average V_{max} forecast error is slightly increased by 2.1% in this situation, which , is trivial but still represents a slight deterioration upon the neutral effect of assimilating all. Combining the effects on P_{min} and $V_{max,}$ CNOP sensitivity displays relatively moderate effect in targeting observation compared to assimilating all, even though the absolute values are trivial for this TC.

3.3.2. *TC Nangka (202016)*

TC Nangka was forecasted to intensify gradually in the CTRL (Fig. 5), which nearly coincides with the BEST in the last 6-h. Compared with TC Higos (202007), the forecast errors are much less for this TC, of which the P_{min} (V_{max}) is within 10 hPa (5 m s^{-1}). Despite the relatively low absolute forecast errors, assimilating all dropsonde data further reduces the P_{min} (V_{max}) forecast error by 13.7% (5.6%). That is, a more accurate intensity forecast is obtained with the help of all dropsonde data. Noting that all dropsondes were released inside the sensitive regions; hence, this positive effect also denotes the benefits CNOP sensitivity brings about.

3.3.3. *TC Saudel (202017)*

The forecast intensities in the CTRL display less obvious variations during the 30-h for TC Saudel (Fig. 5), which maintains a P_{min} (V_{max}) of 985–990 hPa (25–30 m s^{-1}). Such steady intensities deviate significantly from the actual, leading to a corresponding forecast error of 20 hPa (10 m s^{-1}). After assimilating all dropsondes, the forecast P_{min} shows some fluctuations in the former 12-h but generally keeps pace with that in the CTRL. Consequently, including all dropsonde data does not obviously impact the P_{min} forecast for this TC. While for the V_{max} forecast, clear differences occur in the latter 15-h, and the forecast V_{max} in All does not approach the BEST as it does in the CTRL. This increases the forecast error by 13.5% for assimilating all. Combining the behaviors of dropsondes on both P_{min} and V_{max}, it is shown that dropsondes do not benefit the intensity forecast for this TC; and neither does CNOP sensitivity since all dropsondes were released in the CNOP sensitive region.

3.3.4. *TC Atsani (202020)*

The forecast intensities in the CTRL fail to predict the actual intensity for this TC, where a general forecast error of over 20 hPa (10 m s^{-1}) on P_{min} (V_{max}) exists during this 30-h. However, dropsonde data help to produce more accurate intensity forecasts. That is, after assimilating all dropsondes, the forecast errors of P_{min} (V_{max}) are reduced by 5 hPa (2 m s^{-1}), particularly in the latter 12-h, which corresponds to a relative error reduction of 12.5% (12.5%) compared to that in the CTRL. Obviously, the results of P_{min} and V_{max} reveal that dropsondes generally exert a positive effect on the intensity forecast skill for this TC.

The positive effects are also revealed if only seven dropsonde data inside the sensitive region are assimilated. Moreover, such positive effects are comparable to assimilating all on the P_{min} forecast and even greater on the V_{max} forecast. Specifically, seven dropsonde data contribute to a reduction of 12.3% on the P_{min} forecast error, which is only a little less than the 12.5% from All. A reduction of 15.1% on the V_{max} forecast error is also obtained, which is greater than that of 12.5% from All. These results indicate an obvious improvement for the case where dropsondes were released only inside the CNOP sensitive regions.

4. Role of CNOP sensitivity under high resolution

In section 3, the generally positive effects of CNOP sensitivity, compared with assimilating all, are revealed in the OSEs under the same resolution (i.e., 30 km) as they are in identifying the CNOP-sensitive regions. It is well known that finer resolutions contribute to more accurate TC intensity forecasts. This fact inspires us to further evaluate the effects of CNOP sensitivity identified under a coarse resolution on the TC forecasts conducted under a finer resolution. Previous work has shown that CNOP might present different structures under different resolutions, and the major parts of CNOP become increasingly localized with increased horizontal resolution (Zhou and Mu, 2011; 2012). That is, the CNOP sensitive regions identified under a fine resolution usually point to more exact sites. However, these more localized sites are generally covered by those identified under a coarse resolution. Hence, another group of OSEs is produced in double-nested domains, where the sensitive regions identified under coarse resolutions (i.e., 30 km) are still utilized. Specifically, the outer domain exactly covers the same model domain that was used before but with a grid spacing of 15 km. The inner domain is vortex following, which contains 181 × 181 grids, with a grid spacing of 5 km. Both domains share the same parameterization schemes as those under coarse resolutions (see section 2.1), except without cumulus parameterization in the inner domain.

The corresponding results are shown as “Exp-5 km” in

Figs. 4 and 5 in contrast to "Exp-30 km" for the coarse resolution experiment. Compared with those under a coarse resolution, the forecast tracks under a fine resolution are closer to BEST for both TCs Nangka (202016) and Saudel (202017), while the track for TC Atsani (202020) was farther from BEST. These results indicate that the effect of finer resolutions on TC track forecast accuracy is case-dependent. After assimilating all dropsonde data, the average track forecast error is reduced for Nangka (202016) but increased for the other two TCs, Saudel (202017) and Atsani (202020), compared to those in the CTRL respectively (Fig. 4). With further fine-tuning of the estimation of CNOP sensitivity for TCs Higos (202007) and Atsani (202020), it trivially increases the average forecast error by 3.3% for the former, while the effect is nearly neutral by assimilating all; however, the deterioration caused by all dropsonde data for the latter is reduced from 21.2% in All to 17.0% if solely based on CNOP sensitivity. Evidently, the impacts of all dropsondes and CNOP sensitivity on TC track forecast skills under fine resolution are also case-dependent.

Regarding the intensity, the fine resolution helps to obtain more accurate forecasts in the CTRL for TCs Saudel (202017) and Atsani (202020) but not for Nangka (202016) (Fig. 5). However, all dropsondes display general positive

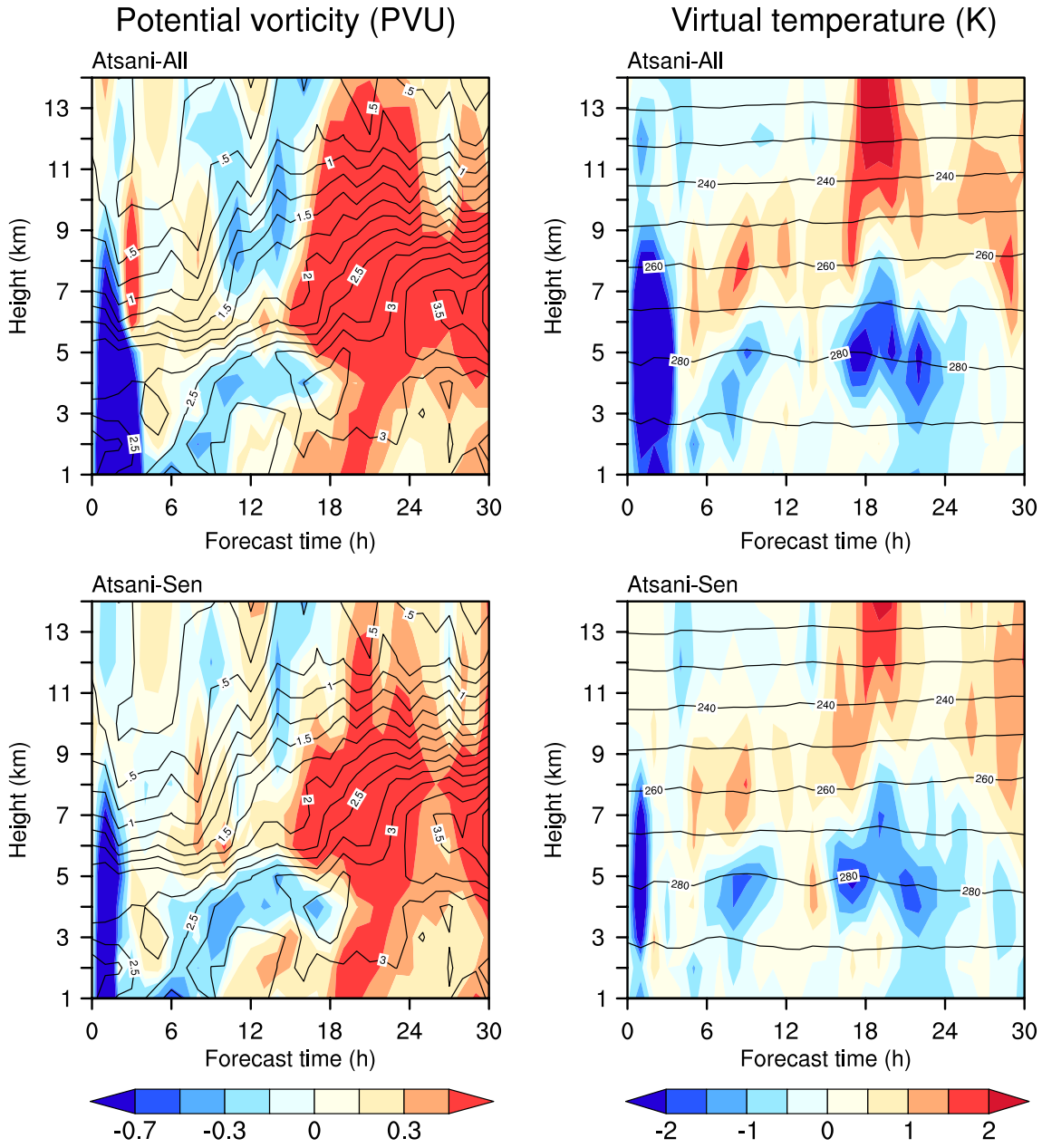

Fig. 6. Left: the differences of time–height cross section of total PV (shaded; PVU) within a radius of 100 km from the individual TC center from that of the CTRL (contours; PVU) for assimilating all dropsonde data (Atsani-All) and some dropsonde data inside the sensitive regions (Atsani-Sen). Right, same as the left but for the averaged virtual temperature (K) within a radius of 40 km from the individual TC center.

effects on the P_{min} forecasts under fine resolutions compared with that under a coarse resolution. They not only bring about reductions in forecast errors for TCs Nangka (202016), Saudel (202017), and Atsani (202020) but also cause much less deterioration than that under coarse resolution for TC Higos (202007). Moreover, the assimilation of the dropsonde data only inside the sensitive regions for TC Higos (202007) further reduces the deterioration to nearly neutral (a slight improvement) for P_{min} (V_{max}) forecasts; and the improvement (deterioration) in P_{min} (V_{max}) forecasts caused by CNOP sensitivity for TC Atsani (202020) is as comparable with (much less than) that of assimilating all. These results indicate that the CNOP sensitivity displays unanimously positive effects on the intensity forecasts compared with assimilating all, even though the CNOP sensitivity is identified under coarse resolution.

Further investigation is conducted into how the inclusion of all dropsondes and CNOP sensitivity influence the intensity forecast skills under a fine resolution. Specifically, the vortex structure [i.e., the total potential vorticity (PV) within a radius of 100 km from the TC center], warm core (i.e., the averaged virtual temperature within a radius of 40 km from the TC center), latent heat, and secondary circulation of the forecasted TCs are compared with and without the assimilation of dropsonde data, as well as those between assimilating all and dropsonde data only inside the CNOP sensitive regions. In general, a forecast TC of stronger intensity exhibits a relatively steady PV and warm core structure with a relatively powerful secondary circulation and latent heat release within the eyewall, and vice versa. That is, the intensity differences in different forecasts for the same TC come from the distinguished forecasted structures of the TC. Taking TC Atsani (202020) as an example, it is shown that both the latent heat and vertical motion in the middle troposphere (i.e., 7–9 km height) are enhanced after assimilating all dropsonde data compared with that in the CTRL (figures are omitted), which contribute greatly to both increasing the PV in the middle troposphere, and increasing the virtual temperature, particularly in the middle and upper troposphere from 12 h on (see Atsani-All in Fig. 6). Consequently, the forecasted TC with the assimilation of all dropsonde data evolves gradually stronger than that of the CTRL and is closer to reality (see Fig. 5). Therefore, P_{min} forecast errors are significantly reduced with the help of all dropsonde data. In addition, the forecasted TC after assimilating the dropsonde data inside the CNOP sensitive region shows a similar secondary circulation, latent heating, and vortex and warm core structures but is a little weaker than those assimilating all [see Atsani-Sen in Fig. 6]. As a result, CNOP sensitivity improves the P_{min} forecasts (see Fig. 5).

Noting that the role of CNOP sensitivity can be better evaluated when both the model identifying the sensitive regions and associated OSEs share the same fine resolution and parameterization schemes. However, in the present study, we cannot achieve this due to the failure of the adjoint check of the WRF model with fine resolutions. Alternatively, the effects of CNOP sensitivity identified under a coarse resolution are evaluated in the OSEs first under coarse and then fine resolutions. The latter will probably weaken the effect of CNOP sensitivity to some degree. However, the advantages of CNOP sensitivity in targeting observation are demonstrated in both groups of OSEs. Nevertheless, developing an advanced method to identify the CNOP sensitivity under fine resolutions is necessary, which can better reveal the sensitive regions for TC intensity forecasts under fine resolutions.

5. Summary and discussion

The field campaigns for TCs over the SCS and WNP were conducted in 2020 and used the CNOP method to identify the sensitive regions for targeting observation following the procedure of the real-time field campaigns for the first time. Within these field campaigns, the HKO and CWB released a certain amount of dropsondes in the environments, occasionally in the eye area, of four TCs: Higos (202007), Nangka (202016), Saudel (202017), and Atsani (202020). Specifically, all the dropsondes were released inside the sensitive regions for TCs Nangka (202016) and Saudel (202017); while for the other two TCs, Higos (202007) and Atsani (202020), only some of them were inside the sensitive regions due to the airspace issue. Most of these dropsondes collected valuable data with a fine vertical resolution, based on which the effects of both dropsonde data and CNOP sensitivity on TC track and intensity forecasts have been evaluated by OSEs.

For the track forecasts, the effects of both dropsonde data and CNOP sensitivity are shown to be case-dependent (see Fig. 7). Assimilating all dropsonde data helps to reduce the track forecast errors for TC Saudel (202017) but shows various negative effects for the other three TCs. For the two TCs with a distribution of dropsonde locations where some were inside, and others were outside the sensitive regions. it is found that assimilating data from a single dropsonde inside the sensitive region for TC Higos (202007) transforms the negative effect caused by assimilating all into a slight positive effect, and the significant deterioration of assimilating all is greatly reduced if only the seven dropsonde data inside the sensitive region are assimilated for TC Atsani (202020). Hence, the CNOP sensitivity behavior is much better than that assimilating all released dropsondes. Nevertheless, it is expected that more data can be obtained from the real-time targeting observations based on the CNOP sensitivity in more field campaigns for TCs in the future, which is helpful for statistical information about the effects of CNOP sensitivity on TC forecast in real-time targeting observation.

Intensity forecasts are also shown to be case-dependent after the assimilation of all dropsondes (see Fig. 7). The forecast skills of P_{min} in TC Atsani (202020) and V_{max} in TCs Nangka (202016) and Atsani (202020) are improved with the contribution of the dropsonde data. However, the impact of CNOP sensitivity on intensity forecasts is unanimously

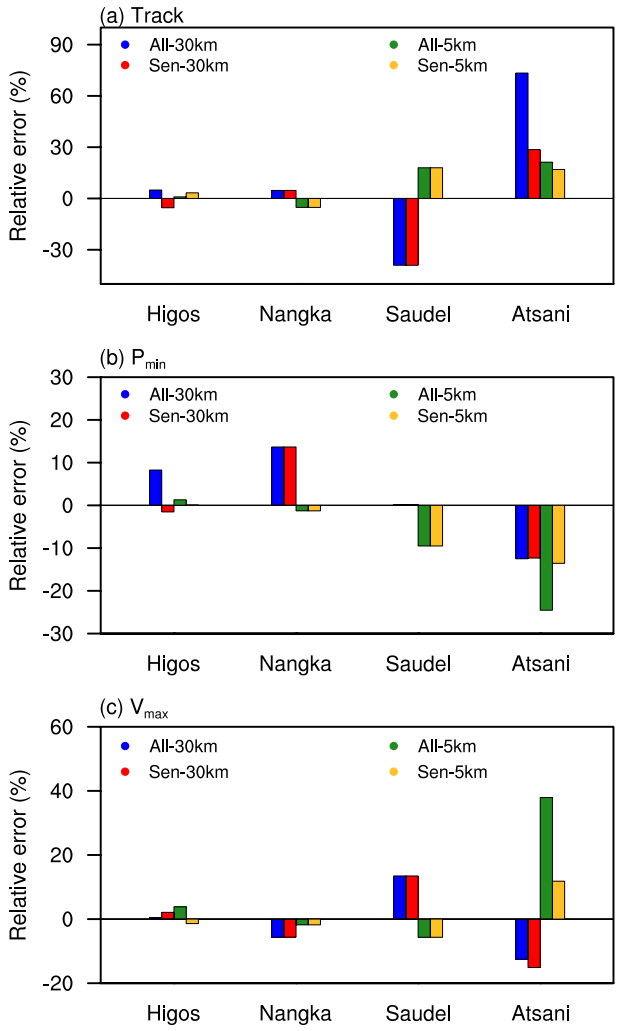

Fig. 7. Averaged reductions of (a) track, (b) P_{min}, and (c) V_{max} forecast errors with respect to the CTRL after assimilating all ("All") released dropsonde data and that in the CNOP sensitive regions ("Sen") using a horizontal resolution of 30 km (blue and red) and 5 km (green and yellow) for four TCs.

more positive than that of assimilating all: comparable or even larger benefits are obtained on both P_{min} and V_{max} forecasts for TC Atsani (202020); moreover, the negative effect on the P_{min} forecast caused by assimilating all for TC Higos (202007) is reversely transformed to positive if the single dropsonde inside the CNOP sensitive region is assimilated, despite a slightly increased forecast error on V_{max}. Moreover, the feasibility of CNOP sensitivity in intensity forecasts is further stressed when utilizing the sensitive regions identified under a coarse resolution to the OSEs under a much finer resolution. Hence, the results in the present study indicate that targeting observation according to the CNOP sensitivity is of great importance in the field campaigns for TC intensity forecasts, especially considering its relatively low forecast skill worldwide. This encourages us to further promote the CNOP method to identify the sensitive regions in targeting observation for TC forecasts.

As the first step in our series of work, the CNOP method has been utilized to identify the sensitive regions following the procedure of the real-time field campaign for TCs in 2020. An important signal is released in this study in that a general positive effect of CNOP sensitivity on TC track and intensity forecasts is found despite the case-dependent nature of their effects. Based on these obtained results, we are encouraged to collaborate closely with field campaigns to collect additional observations for more TCs in the future. Meanwhile, we are trying to resolve some technical issues related to designing the flights for launching dropsondes more effectively and calculating the CNOP sensitivity under finer resolutions without an adjoint model. With a large amount of TC observations, we hope to statistically reveal general rules associated with the following concerns: (1) what are the characteristics of CNOP-sensitive regions with relatively high and low sensitivity; (2) which type of TCs benefit the most from targeting observations; (3) why reverse effects of targeting observation occur during different stages for the same TC. It is expected that these related work will offer great promise in improving the forecast skill of TCs.

Acknowledgements. The authors appreciate the anonymous reviewers very much for their insightful comments and suggestions. This work was jointly sponsored by the National Nature Scientific Foundation of China (Grant. Nos. 41930971 and 41775061) and the National Key Research and Development Program of China (Grant No. 2018YFC1506402).

Data Availability Statement: The forecasts from the European Centre for Medium-Range Weather Forecasts were taken from the following source: https://apps.ecmwf.int/datasets/data/tigge/levtype=sfc/type=cf/. The dropsonde data were from the Hong Kong Observatory and the Central Weather Bureau. These data are available on request.

REFERENCES

Aberson, S. D., 2010: 10 years of hurricane synoptic surveillance (1997–2006). *Mon. Wea. Rev.*, **138**, 1536–1549, https://doi.org/10.1175/2009MWR3090.1.

Birgin, E. G., J. M. Martínez, and M. Raydan, 2001: Algorithm 813: SPG—Software for convex-constrained optimization. *ACM Transactions on Mathematical Software*, **27**, 340–349, https://doi.org/10.1145/502800.502803.

Black, P., L. Harrison, M. Beaubien, R. Bluth, R. Woods, A. Penny, R. W. Smith, and J. D. Doyle, 2017: High-Definition Sounding System (HDSS) for atmospheric profiling. *J. Atmos. Oceanic Technol.*, **34**, 777–796, https://doi.org/10.1175/JTECH-D-14-00210.1.

Braun, S. A., P. A. Newman, and G. M. Heymsfield, 2016: NASA's hurricane and severe storm sentinel (HS3) investigation. *Bull. Amer. Meteor. Soc.*, **97**, 2085–2102, https://doi.org/10.1175/BAMS-D-15-00186.1.

Burpee, R. W., J. L. Franklin, S. J. Lord, R. E. Tuleya, and S. D. Aberson, 1996: The impact of Omega dropwindsondes on operational hurricane track forecast models. *Bull. Amer. Meteor. Soc.*, **77**, 925–933, https://doi.org/10.1175/1520-0477(1996)077<0925:TIOODO>2.0.CO;2.

Chen, B. Y., M. Mu, and X. H. Qin, 2013: The impact of assimilat-

ing dropwindsonde data deployed at different sites on typhoon track forecasts. *Mon. Wea. Rev.*, **141**, 2669–2682, https://doi.org/10.1175/MWR-D-12-00142.1.

Chou, K.-H., C.-C. Wu, P.-H. Lin, S. D. Aberson, M. Weissmann, F. Harnisch, and T. Nakazawa, 2011: The impact of dropwindsonde observations on typhoon track forecasts in DOTSTAR and T-PARC. *Mon. Wea. Rev.*, **139**, 1728–1743, https://doi.org/10.1175/2010MWR3582.1.

Feng, J., and X. G. Wang, 2019: Impact of assimilating upper-level dropsonde observations collected during the TCI field campaign on the prediction of intensity and structure of hurricane Patricia (2015). *Mon. Wea. Rev.*, **147**, 3069–3089, https://doi.org/10.1175/MWR-D-18-0305.1.

Feng, J., X. H., Qin, C. Q., Wu, P., Zhang, L., Yang, X. S., Shen, W., Han, and Y. Z., Liu, 2022: Improving typhoon predictions by assimilating the retrieval of atmospheric temperature profiles from the FengYun-4A's geostationary interferometric infrared sounder (GIIRS). *Atmospheric Research*, 280, https://doi.org/10.1016/j.atmosres.2022.106391.

Hong, S. Y., T. Noh, and J. Dudhia, 2006: A new vertical diffusion package with an explicit treatment of entrainment processes. *Mon. Wea. Rev.*, **134**, 2318–2341, https://doi.org/10.1175/MWR3199.1.

Iacono, M. J., J. S. Delamere, E. J. Mlawer, M. W. Shephard, S. A. Clough, and W. D. Collins, 2008: Radiative forcing by long-lived greenhouse gases: Calculations with the AER radiative transfer models. *J. Geophys. Res.*, **113**(D13), D13103, https://doi.org/10.1029/2008JD009944.

Kain, J. S., and J. M. Fritsch, 1993: Convective parameterization for mesoscale models: The Kain-Fritsch scheme. *The Representation of Cumulus Convection in Numerical Models*, K. A. Emanuel and D. J. Raymond., Eds., American Meteorological Society, 165–170, https://doi.org/10.1007/978-1-935704-13-3_16.

Lin, Y. L., R. D. Farley, and H. D. Orville, 1983: Bulk parameterization of the snow field in a cloud model. *J. Appl. Meteorol. Climatol.*, **22**, 1065–1092, https://doi.org/10.1175/1520-0450(1983)022<1065:BPOTSF>2.0.CO;2.

Mu, M., W. S. Duan, and B. Wang, 2003: Conditional nonlinear optimal perturbation and its applications. *Nonlinear Processes in Geophysics*, **10**, 493–501, https://doi.org/10.5194/npg-10-493-2003.

Mu, M., F. F. Zhou, and H. L. Wang, 2009: A method for identifying the sensitive areas in targeted observations for tropical cyclone prediction: Conditional nonlinear optimal perturbation. *Mon. Wea. Rev.*, **137**, 1623–1639, https://doi.org/10.1175/2008MWR2640.1.

Qin, X. H., and M. Mu, 2012: Influence of conditional nonlinear optimal perturbations sensitivity on typhoon track forecasts. *Quart. J. Roy. Meteor. Soc.*, **138**, 185–197, https://doi.org/10.1002/qj.902.

Qin, X. H., W. S. Duan, and H. Xu, 2020: Sensitivity to tendency perturbations of tropical cyclone short-range intensity forecasts generated by WRF. *Adv. Atmos. Sci.*, **37**, 291–306, https://doi.org/10.1007/s00376-019-9187-6.

Snyder, C., 1996: Summary of an informal workshop on adaptive observations and FASTEX. *Bull. Amer. Meteor. Soc.*, **77**, 953–961, https://doi.org/10.1175/1520-0477-77.5.953.

Weissmann, M., and Coauthors, 2011: The influence of assimilating dropsonde data on typhoon track and midlatitude forecasts. *Mon. Wea. Rev.*, **139**, 908–920, https://doi.org/10.1175/2010MWR3377.1.

Wu, C.-C., and Coauthors, 2005: Dropwindsonde observations for typhoon surveillance near the Taiwan region (DOTSTAR): An overview. *Bull. Amer. Meteor. Soc.*, **86**, 787–790, https://doi.org/10.1175/BAMS-86-6-787.

Wu, C.-C., K.-H. Chou, P.-H. Lin, S. D. Aberson, M. S. Peng, and T. Nakazawa, 2007: The impact of dropwindsonde data on typhoon track forecasts in DOTSTAR. *Wea. Forecasting*, **22**, 1157–1176, https://doi.org/10.1175/2007WAF2006062.1.

Zhou, F. F., and M. Mu, 2011: The impact of verification area design on tropical cyclone targeted observations based on the CNOP method. *Adv. Atmos. Sci.*, **28**(5), 997–1010, https://doi.org/10.1007/s00376-011-0120-x.

Zhou, F. F., and M. Mu, 2012: The impact of horizontal resolution on the CNOP and on its identified sensitive areas for tropical cyclone predictions. *Adv. Atmos. Sci.*, **29**(1), 36–46, https://doi.org/10.1007/s00376-011-1003-x.